

Graphene Oxide/Zinc Oxide (GO/ZnO) Nanocomposite as a Superior Photocatalyst for Degradation of Methylene Blue (MB)-Process Modeling by Response Surface Methodology (RSM)

Seyed A. Hosseini* and Shabnam Babaei

Department of Applied Chemistry, Faculty of Chemistry, Urmia University, Urmia, Iran

The photocatalytic performance of graphene oxide/zinc oxide (GO/ZnO) nanocomposite was investigated for degradation of methylene blue (MB) from wastewater and was compared with that of zinc oxide (ZnO), graphene oxide (GO) and carbon nanotube/zinc oxide (CNT/ZnO). The properties of the GO/ZnO nanocomposite were characterized by X-ray diffraction (XRD), Fourier transform infrared (FTIR), scanning electron microscopy (SEM) and transmission electron microscopy (TEM). The SEM and TEM results revealed the nanostructure of the composite. The photocatalytic process was modeled by response surface methodology (RSM), considering four independent factors. The significance of the model was approved by analysis of variance (ANOVA) (determination coefficient $R^2 = 0.95$, $R^2_{adj} = 0.91$). The optimum conditions of the process were found to be at photocatalyst dosage, initial pH, H_2O_2 concentration and irradiation time of 2.1 g L^{-1} , 4.5, $3.5 \times 10^{-4} \text{ mol L}^{-1}$ and 140 min, respectively. The removal of MB over GO/ZnO was 99% under the optimum conditions and was superior than that over GO and CNT/ZnO. According to Pareto analysis of the modeling, the irradiation time and photocatalyst dosage were the most effective factors on the decolorization efficiency of methylene blue, respectively.

Keywords: photocatalyst, nanocomposite, graphene oxide, response surface methodology, dye removal

Introduction

The presence of organic dye in aqueous environments can cause detrimental effects on aquatic life and subsequently human health.¹ Photocatalysis, one of advanced oxidation processes (AOPs), is an efficient technique for water and air purification due to its several advantages.² Zinc oxide (ZnO), with a large band gap (3.37 eV), is one of the most popular photocatalysts due to its chemical stability, non-toxicity nature and high photocatalytic activity in the removal of pollutants in water or air.³ Despite its great potential, the photocatalytic efficiency of ZnO has been often low because of the fast recombination of the photogenerated electron-hole pairs and the limited photoresponding range. Therefore, various strategies, including structural design, noble metal loading, ion doping, and the coupling of semiconductors, have been proposed to extend the light absorption range or suppress the electron-hole recombination of ZnO.⁴ Carbonaceous materials are of tremendous interest due to

their unique pore structure, electronic properties, adsorptive capacity and acidity. These materials include activated carbon, carbon nanotubes and graphene.⁵ In comparison to carbon nanotubes (CNTs), graphene has the perfect sp^2 hybrid carbon nanostructure and the high specific surface area, which can be easily obtained from natural graphite via a facile chemical oxidation-exfoliation-reduction procedure at a low cost.⁶ One of the most well-developed applications of graphene based materials is the removal of pollutants from water through technologies such as adsorption and photocatalytic degradation.⁷ It is expected that the combination of ZnO with graphene may be ideal to have superior photocatalytic performance because of the conjugated structure of graphene which facilitates the charge separation in the photocatalysis process.⁵ Meanwhile, graphene oxide (GO) is receiving increasing attention because it possesses the similar properties to graphene as well as the special surface structures with the introduced hydroxyl and carboxyl groups for the synthesis of GO-containing nanocomposites.⁸

A considerable number of articles have been published regarding removal of harmful compounds from water,

*e-mail: s_ali_hosseini@yahoo.com, a.hosseini@urmia.ac.ir

wastewater and air, using photocatalytic methods, which imply the importance of the mentioned method in removing pollutants.⁸⁻¹⁴ There are various reports¹⁵⁻¹⁸ on the application of ZnO and TiO₂ nanoparticles as photocatalysts for the degradation of dyes using response surface methodology. Furthermore, in some of the articles, the photocatalytic degradation of methylene blue (MB) by ZnO/graphene, ZnO nanoparticles NPs/rGO and ZnO/rGO composites have been investigated.^{5,19,20}

In this work, GO/ZnO nanocomposite was synthesized and photocatalytic process of MB removal from wastewater under UV irradiation by GO/ZnO nanocomposite was investigated. The response surface methodology (RSM) was employed to assess individual and interactive effects of the four main independent parameters (photocatalyst dosage, initial pH, H₂O₂ concentration and irradiation time) on the removal efficiency of MB. Box-Behnken design was used for optimization of photocatalytic process. The nanocomposite was characterized by X-ray diffraction (XRD), Fourier transform infrared (FTIR), scanning electron microscopy (SEM) and transmission electron microscopy (TEM).

Experimental

Materials

All reagents, except multi walled carbon nanotubes, were purchased from Merck Co. (Germany) and used as received. Graphite powder was obtained from the brain of old batteries to recycling of waste.

Carbon nanotube (CNT) was obtained from Chengdu Organic Chemicals Co. (China). Table 1 presents the characteristic data of CNT.

Table 1. Characteristic properties of CNT

Factor	Value	entry
Outer diameter (OD) / nm	20-40	1
Length / μm	ca. 30	2
Purity / (wt.%)	> 85	3
Ash / (wt.%)	< 8	4
Specific surface area / ($\text{m}^2 \text{g}^{-1}$)	> 100	5

Synthesis of GO

GO was synthesized using natural graphite by the modified Hummers method.²¹ In a typical synthesis, 2 g of graphite powder was added into 46 mL of 98% H₂SO₄ under continuous stirring for 1 h at 0 °C in an ice bath. At the given intervals, 1 g of NaNO₃ and 6 g of KMnO₄ were

added slowly to the above solution within 2 h. Afterwards, the solution was stirred for 2 h at 25 °C before diluting with 280 mL distilled water. Then, 6 mL of hydrogen peroxide was added to remove KMnO₄ excess. The observed color of the mixture was a dark yellow. The resulting product was filtered, then the mixture was washed with distilled water until the pH became 7 and dried at 60 °C under vacuum. The GO was then dispersed in distilled water to make concentration of 1 g L⁻¹ and exfoliated by ultrasonication for 3 h to obtain GO nanosheets.

Synthesis of ZnO

In order to synthesis of ZnO nanoparticles, sodium hydroxide solution was added dropwise to the aqueous solution of zinc sulfate in a molar ratio of 1:2 and left stirring for 12 h. ZnO nanoparticles were formed and precipitated at the bottom of the solution. The obtained precipitate was filtered and washed thoroughly with distilled water. The precipitate was dried in an oven at 100 °C.²² The white powder obtained from the above method was calcined at 300 °C for 2 h.

Synthesis of GO/ZnO

GO was dissolved into ethanol and kept under ultrasonication for 2 h and it was denoted as GO solution. The as-prepared ZnO nanoparticles were dissolved into the mixture of methanol and chloroform and kept under ultrasonication for 2 h and denoted as ZnO solution. Usually the ratio of methanol over chloroform is about 8-9. The volumetric ratio of the two solvents could be adjusted to dissolve all the ZnO nanoparticles to obtain clear solution. The GO solution and the ZnO solution were mixed and kept under constant stirring for 24 h. The collected precipitate was obtained by centrifugation and washed with methanol for several times. The product was freeze dried overnight and denoted as GO-ZnO nanocomposites.²³

Determination of pH_{PZC} of the adsorbents

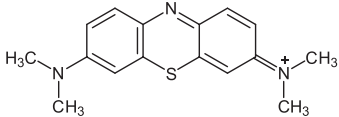
The point of zero charge (pH_{PZC} values) is the point at which the net charge on the adsorbent surface is zero. The pH_{PZC} values of GO and GO/ZnO was determined by pH drift method.²⁴ Briefly, several solutions containing 0.01 mol L⁻¹ NaCl were supplied. The initial pH (pH_i) of the solutions was adjusted to a value between 2 and 11 using 0.1 mol L⁻¹ HCl or NaOH. 0.02 g adsorbent was added to the solution. The electrolyte solution with adsorbent was equilibrated for 24 hours. After equilibrium, the final pH (pH_f) was recorded. The pH_f was plotted against the

initial pH (pH_i) values. The pH at which pH_i crosscovered the (pH_f) was referred to as the pH_{PZC} . The pH_{PZC} of GO and GO/ZnO was determined 7.5 and 8.2, respectively.

Photocatalysis experiments

Photocatalytic activities of the synthesized GO/ZnO nanocomposite were evaluated by the degradation of MB under UV irradiation (by a 15 W UV lamp, Philips, Netherlands). As approved in literature, the initial concentration of dye exhibits an inverse relationship with removal efficiency of dye. So we did not consider it as a factor in our study. Therefore, in all experiment the concentration of dye was considered 10 ppm. In each experiment, the special amount of photocatalyst was poured into 100 mL MB (10 ppm). The suspension was initially stirred in the dark for 30 min to ensure adsorption equilibrium before exposing it to UV irradiation for different times. Then the suspension was exposed to UV illumination. At given times during the process, 3 mL of the solutions were taken and centrifuged to remove the particles. The concentration of the MB solutions was determined at $\lambda_{max} = 664$ nm by a PG instrument T80+ spectrophotometer. The properties of MB used in this research are presented in Table 2.

Table 2. Characteristics of methylene blue (MB) dye

Chemical structure	
Type of dye	cationic
Symbol	MB
Molecular formula	$C_{16}H_{18}N_3S$
Molecular weight / ($g\ mol^{-1}$)	319.85
Maximum absorption wavelength / nm	664

Experimental design, statistical analysis and optimization by response surface methodology (RSM)

Response surface methodology (RSM) is a set of mathematical and statistical tools for designing experiments, modeling, evaluating the effects of the factors and researching the optimal values of factors to predict target responses. To reduce the number of experiments, arranging the experiments with various combinations of independent variables and optimization study of the photocatalytic process Box-Behnken design under response surface methodology (RSM) was employed.

The use of Box-Behnken design is popular in industrial research because it is an economical design and requires only three levels (-1, 0, 1) for each factor. This design is useful in avoiding experiments that would be performed under extreme conditions, for which unsatisfactory results might occur.²⁵ The number of experiments required (N) is given by:

$$N = 2k(k - 1) + C_0 \quad (1)$$

where k is the number of variables and C_0 is the number of central points (here is 3).

In this study, four independent variables were considered: photocatalyst dosage ($g\ L^{-1}$) (X_1), pH (X_2), H_2O_2 concentration ($\times 10^{-4}\ mol\ L^{-1}$) (X_3) and irradiation time (min) (X_4). Table 3 presents the ranges and levels of independent variables. The ranges of the independent variables were determined by considering the literature. All experiments for modeling were run based on the experimental design matrix (Table 4).

In the RSM, a second order polynomial equation is usually applied to correlate the dependent and independent variables:

$$Y = b_0 + b_i X_i + b_{ii} X_i^2 + b_{ij} X_i X_j + \varepsilon \quad (2)$$

where Y_i is the response, b_0 is the constant, b_i is the slope or linear effect of the input factor, b_{ii} is the quadratic effect, b_{ij} is the two-way linear by linear interaction effect, X_i and X_j are the independent parameters and ε is the random error. Equation 2 expresses the relationship between the predicted response and the independent variables in coded values.²⁵

Table 3. Independent variables and their coded levels and actual values

Independent variable	Symbol	Range and level		
		Low (-1)	Middle (0)	High (+1)
Photocatalyst dosage / ($g\ L^{-1}$)	X_1	0.1	1.1	2.1
pH	X_2	3.5	4.5	5.5
$[H_2O_2] (\times 10^{-4}) / (mol\ L^{-1})$	X_3	1	3.5	6
Irradiation time / min	X_4	20	80	140

Results and Discussion

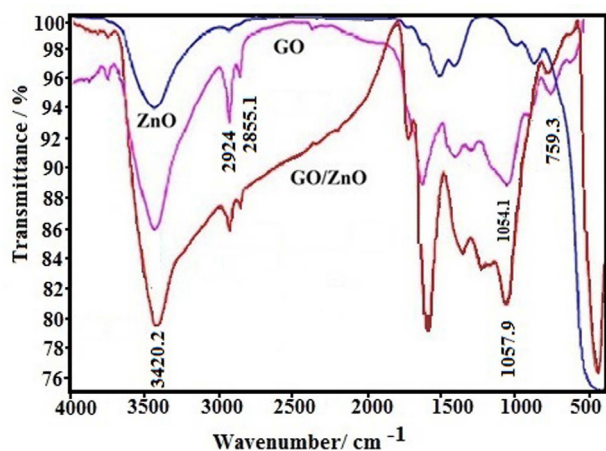
Characterization

Figure 1 shows the FTIR spectra of the GO, ZnO and GO/ZnO nanocomposites. In the FTIR spectrum of the GO sample, the main absorption band at $3430\ cm^{-1}$ is assigned to the O-H group stretching vibrations. The

Table 4. Box-Behnken design with predictive values and their experimental results

Run	Photocatalyst dosage / (g L ⁻¹)	pH	[H ₂ O ₂] (× 10 ⁻⁴) / (mol L ⁻¹)	Irradiation time / min	Percentage removal of methylene blue	
					Experimental	Predictive
1	0	1	0	1	74	71.95
2	-1	0	-1	0	22	22.06
3	0	-1	0	-1	30	25.7
4	1	0	0	-1	36	34.26
5	0	0	1	-1	48	55.51
6	0	0	1	1	88	95.51
7	0	1	0	-1	39	36.95
8	0	0	0	0	42	39.77
9	0	1	1	0	84	79.82
10	1	0	-1	0	80	76.32
11	1	-1	0	0	66	67.7
12	-1	0	0	-1	21	24.76
13	0	-1	1	0	70	73.57
14	0	-1	0	1	75	70.7
15	0	-1	-1	0	37	47.87
16	1	1	0	0	57	66.2
17	0	0	0	0	36	39.77
18	-1	0	1	0	81	70.33
19	1	0	0	1	99	97.26
20	0	0	-1	-1	33	29.81
21	0	1	-1	0	55	54.12
22	1	0	1	0	84	80.25
23	-1	1	0	0	41.5	41.45
24	0	0	-1	1	73	69.81
25	0	0	0	0	36	39.77
26	-1	0	0	1	38	41.76
27	-1	-1	0	0	35	27.45

absorption peak at 1627 cm⁻¹ can be assigned to C=O stretching of carboxylic and/or carbonyl moiety functional groups. The peaks at 1054.10 and 918.51 cm⁻¹ are assigned to the stretching of C–OH and C–O, respectively. The peaks around 2924.24 and 2855.15 cm⁻¹ can be assigned to the asymmetric and symmetric vibrations of C–H,

**Figure 1.** FTIR spectra of ZnO, GO, GO-ZnO nanocomposites.

respectively. The broad peak at 3420.24 cm⁻¹ in the FTIR spectrum of the GO/ZnO nanocomposite might be attributed to the O–H stretching vibration of the C–OH groups and water. In addition, the strong absorption band in the range of < 500 cm⁻¹ is corresponding to the vibrations of Zn–O bonds.

The XRD patterns of ZnO nanoparticles and GO/ZnO nanocomposite are shown in Figures 2a and 2b, respectively.

In the XRD pattern of the ZnO nanoparticles (Figure 2a), the peaks at 32, 34.6, 36.4, 47.8, 56.8, 63, 68.3, 69.53 and 77.5 correspond to (110), (002), (101), (102), (110), (103), (112), (201) and (202) crystalline planes of ZnO, respectively.^{5,8,20} The main peaks of the XRD pattern of GO/ZnO nanocomposite are shown in Figure 2b. The diffraction peaks of GO/ZnO nanocomposite are similar to those of ZnO nanoparticles and the main peaks of ZnO are observed in the XRD pattern of the nanocomposite. The peak around 2θ = 10–15° is assigned to graphene oxide nanosheet. The GO peak in the nanocomposite suggests that the nanocomposite sheets restacked.

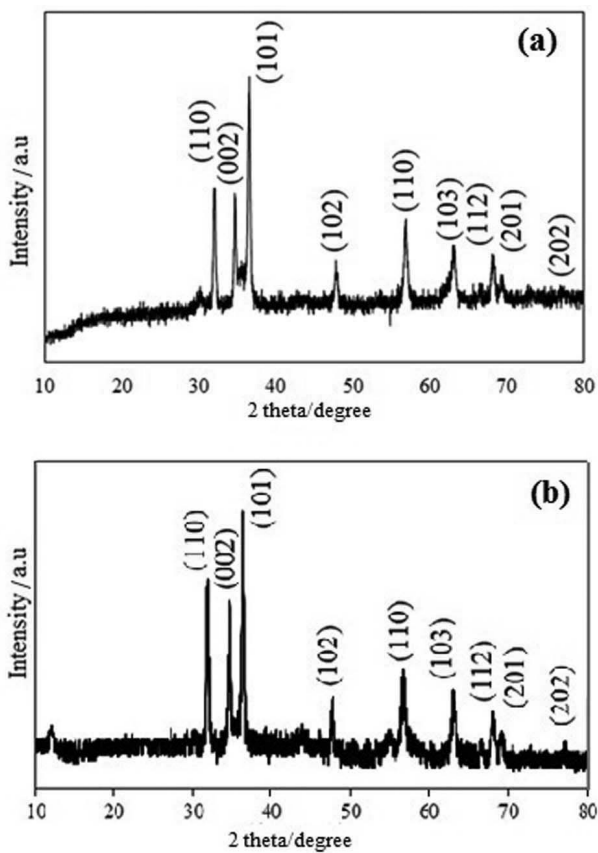


Figure 2. XRD plot for (a) ZnO and (b) GO/ZnO nanocomposite.

To investigate the surface morphology and particle size of GO/ZnO composite, SEM images were taken and presented in Figure 3. Figure 3a shows the particles of ZnO have been dispersed on graphene oxide sheets. It is observed that some ZnO particles have been agglomerated. Figure 3b shows the particle size of ZnO dispersed on graphene sheet. The diameter of ZnO particles is less than 100 nm and the diameter of the two particles are determined 82.04 and 98.21 nm.

The representative TEM images of GO and GO/ZnO composite are shown in Figures 4a and 4b, respectively. A large graphene oxide sheet with dimension of nanometers has been found to be situated on the top of the grid (Figure 4a), where it shows transparent and rippled silk wave appearances. The wrinkles and folded parts are attributed to graphene oxide. In the case of the TEM image of GO/ZnO (Figure 4b), the small spots dispersed on the graphene oxide flake is attributed to the ZnO nanoparticles. So, both images approve the nanosheet of GO and nanoparticles on ZnO in the composite.

From the different models evaluated, the following quadratic response surface model (equation 3) could best fit the experimental results among different evaluated models:

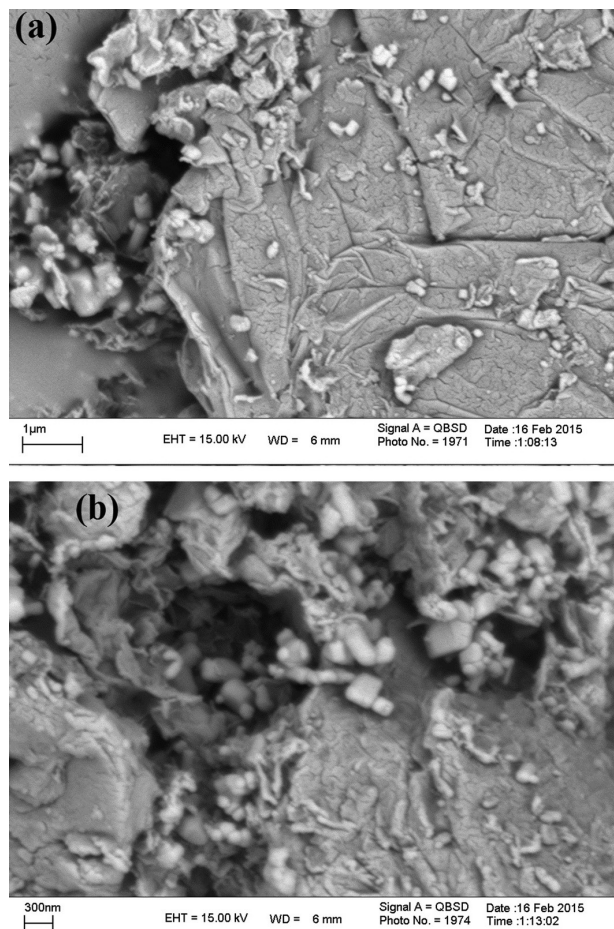


Figure 3. SEM images of GO/ZnO nanocomposite. The scale bars in the images of (a) and (b) are 1 µm and 300 nm, respectively.

$$Y = 44.12 + 16.10X_1 + 3.12X_2 + 12.79X_3 + 20X_4 + 3.19X_1^2 + 4.77X_2^2 + 16.01X_3^2 - 3.87X_1X_2 - 11.34X_1X_3 + 11.50X_1X_4 \quad (3)$$

The sign of independent factors is positive in the model, indicating that all the independent factors have a synergistic effect on the response.

Photocatalytic efficiencies of MB removal (Y) have been predicted by equation 3 and presented in Table 4. These results indicated good agreements between the experimental and predicted values of decolorization efficiency.

The suitability of a model is evaluated by analysis of variance (ANOVA). The results of ANOVA for the model is presented in Table 5.

The significance of the model was evaluated by the determination coefficient (R^2). Figure 5 shows the plot of the model predicted responses *versus* response. It is observed that the R^2 value means an acceptable agreement between the experimental and predicted values of the fitted data ($R^2 = 0.95$). The closer the R^2 (value = 1), the stronger

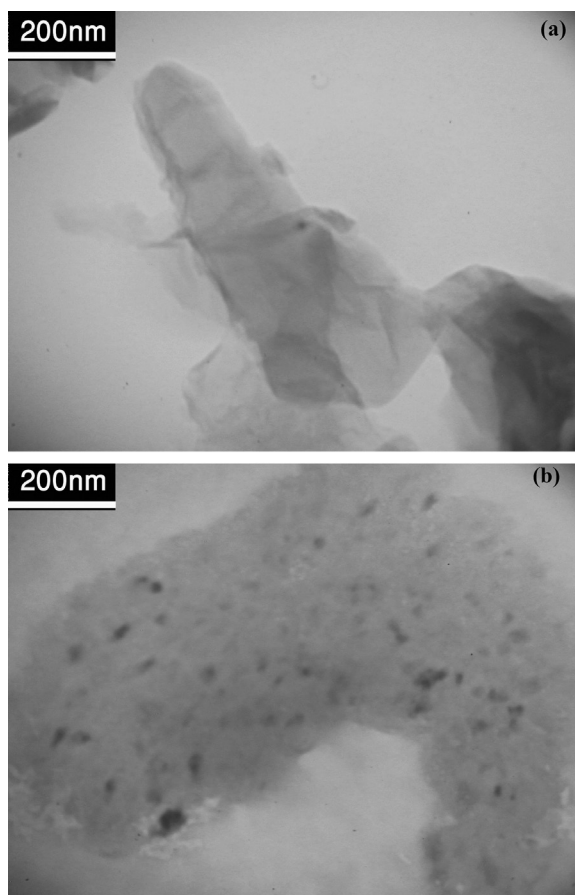


Figure 4. TEM images of (a) GO and (b) GO/ZnO nanocomposite.

the model is and the better it predicts the response.²⁶ Adjusted R^2 (R^2_{adj}) is also a measure of the goodness of a fit, but it is more suitable for comparing models with different numbers of independent variables.²⁷ The adjusted R^2 was 0.91 for the model. The difference of R^2_{adj} and R^2_{pred} value was less than 0.2 (20%), indicating the significance of the model. In addition, the Fisher's F-test was used to verify the statistical significance of the model.

The greater the F-value is from unity, the more certain it is that the factors explain adequately the variation in the data about its mean, and the estimated factor effects are real. The probability p -value is relatively low, indicating the significance of the model.²⁶ In this study, a very high F-value ($F_{model} = 23.75$, much greater than unity) and a very low probability value ($p_{model} = 0.000$) confirms highly significant of the model (see Table 5).

Table 5. Analysis of variance (ANOVA) for decolorization of MB by the photocatalytic process

Source of variations	Degree of freedom	Sum of squares	Adjusted mean square	F-value	p -value
Regression	10	12693.5	1269.35	23.75	0.000
Residuals	16	885.0	53.44	–	–
Total	26	13548.5	–	–	–

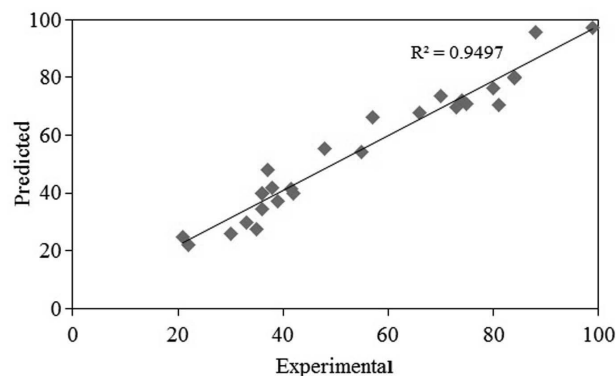


Figure 5. Comparison of predicted response of degradation with experimental response.

On the other hand, the significance of the regression coefficient of the model terms was investigated by p -value and t -value.

The p -values were used as a tool to check the significance of each of the coefficients, which in turn, are necessary to understand the pattern of the mutual interactions between the test variables.²⁸ The larger the magnitude of the t -value and the smaller the p -value, the more significant the corresponding coefficient.¹⁵ The p -value and t -value of the each coefficient are presented in Table 6.

The coefficients of the linear effect of catalyst dosage, H_2O_2 concentration and irradiation time with p -value of zero were significant, whereas the coefficient of pH is not at a confidence level of 95% (p -value ≤ 0.05). In the case of quadratic effects of (X_1^2), just the coefficient of $C_{H_2O_2}$ - $C_{H_2O_2}$ (X_3^2) was significant at the confidence level of 95% and the term X_4^2 was removed from the model. In the case of binary terms, the interactions of X_1X_3 and X_1X_4 were significant at a confidence level of 95% (p -value ≤ 0.05).

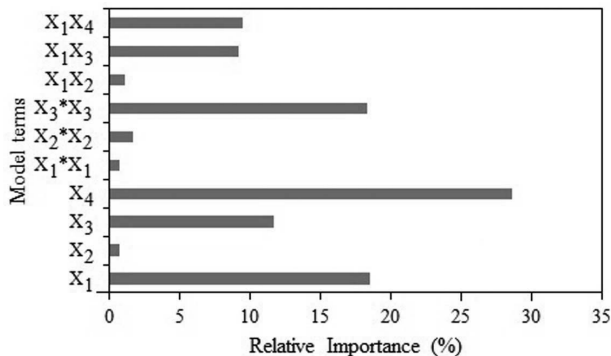
The Pareto analysis gives more significant information to interpret the results. In fact, this analysis calculates the percentage effect (relative importance) of each factor on the response, according to the following relation:¹⁶

$$p_i = \left(\frac{b_i^2}{\sum b_i^2} \right) \times 100 \quad (i \neq 0) \quad (4)$$

Pareto analysis graphic analyses are summarized in Figure 6. As can be seen in this figure, the order of relative

Table 6. Estimated regression coefficients and corresponding *t*- and *p*-values from the data of Box-Behnken design experiments

Coefficient	Standard error	<i>t</i> -value	<i>p</i> -value
b_0	372	7.97	0
b_1	293	3.02	0.008
b_2	27	1.55	0.141
b_3	54.2	5.19	0
b_4	272	7.19	0
b_{11}	3.17	1.01	0.329
b_{22}	2.96	1.61	0.126
b_{33}	19.5	5.12	0
b_{12}	3.65	-1.06	0.305
b_{13}	11.4	-2.48	0.025
b_{14}	219	3.15	0.006

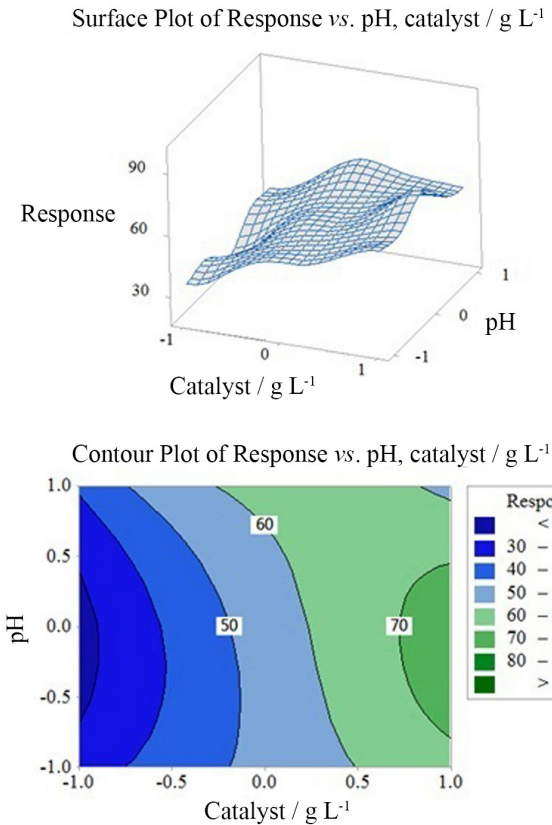
**Figure 6.** Pareto graphical analysis.

importance of variables in photocatalytic decolorization efficiency is as follows: irradiation time (X_4) > photocatalyst dosage (X_1) > H_2O_2 concentration (X_3) > pH (X_4).

In order to achieve better understanding of the interactions between factors and to determine the optimum level of each factor for maximum response 3D surface plot and 2D contour plots were used. Figures 7a and 7b shows the surface plot and contour plot for combined interaction of catalyst dosage and pH, respectively.

From these figures, it was found that pH has negative effects when being coupled with adsorbent dosage (X_1). This was evidenced from the positive terms in equation 3 and also the convex response surfaces that indicate well-defined optimum variables. Maximum response results in high level of X_1 and medium level of X_2 (pH = 4.5).

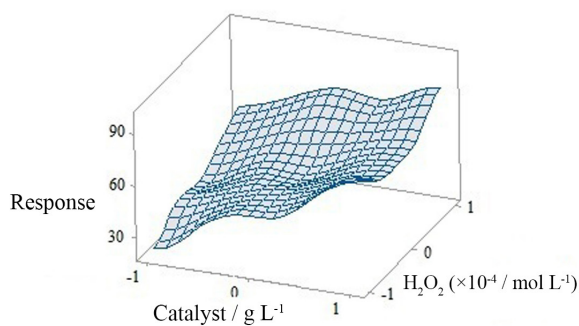
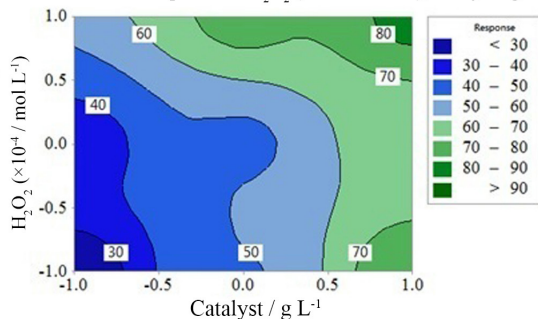
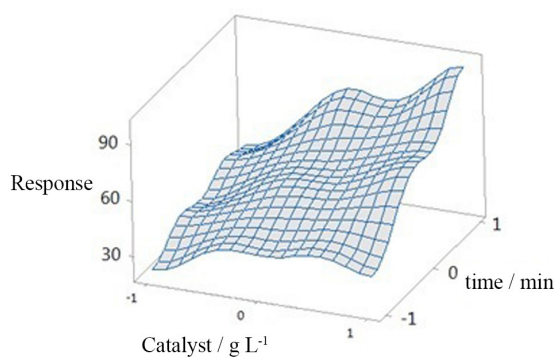
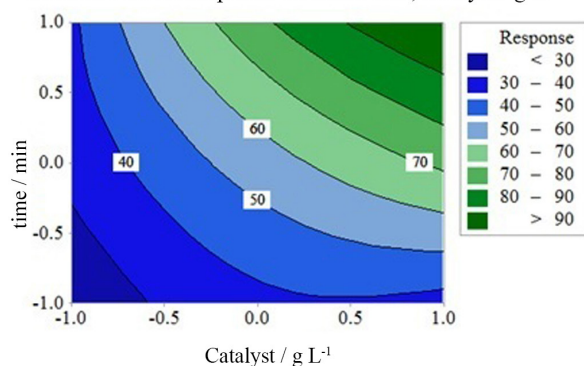
The interaction of catalyst dosage (X_1) and X_3 (H_2O_2 concentration) on the response has been investigated by surface plot and contour plot as shown in Figure 8. It is observed that the increasing of catalyst dosage and H_2O_2 concentration increased the response of the model

**Figure 7.** The surface plots and contour plots of the decolorization efficiency (CR%) as the function of catalyst dosage and pH.

and maximum MB removal occurs at both high levels of both factors.

Regarding the effect of irradiation time and catalyst dosage on the removal of MB efficiency, as can be seen in Figure 9, the removal of MB efficiency increases by the increasing of the irradiation time and catalyst dosage, respectively.

Furthermore, the developed model predicted the optimum conditions to get high efficiency for decolorization. The conditions are presented in Table 7. For these conditions, the model predicted the efficiency of 97.3%, whereas the experimental test in optimum conditions resulted 99% removal of MB, implying that this model is useful to optimize the decolorization conditions and to obtain the best conditions by the modeled formula. In addition to GO/ZnO nanocomposite, the photocatalytic performance of ZnO, GO, CNT and CNT/ZnO were tested and the results of MB degradation on these materials are presented in Table 8. It is resulted that other photocatalysts show high activity under optimum catalyst. GO exhibits photocatalytic activity, but carbon nanotube is not a photocatalyst. It is resulted that the most portion of photocatalytic behavior is due to ZnO.

Surface Plot of Response vs. H_2O_2 ($\times 10^{-4}$ / mol L^{-1}), catalyst / g L^{-1} Contour Plot of Response vs. H_2O_2 ($\times 10^{-4}$ / mol L^{-1}), catalyst / g L^{-1} **Figure 8.** The surface plots and contour plots of the decolorization efficiency (CR%) as the function of catalyst dosage and H_2O_2 concentration.Surface Plot of Response vs. time / min, catalyst / g L^{-1} Contour Plot of Response vs. time / min, catalyst / g L^{-1} **Figure 9.** The surface plots and contour plots of the decolorization efficiency (CR%) as the function of catalyst dosage and irradiation time.**Table 7.** Optimum values of the parameters for 99% decolorization efficiency by the process

Parameter	Optimum value
Photocatalyst dosage (X_1) / (g L^{-1})	2.1
Initial pH (X_2)	4.5
$[\text{H}_2\text{O}_2]$ ($\times 10^{-4}$) / (mol L^{-1})	3.5
Irradiation time (X_4) / min	140

Table 8. The removal percent of MB over different photocatalysts under optimum conditions

Photocatalyst	Methylene blue degradation / %
GO/ZnO nanocomposite	99
ZnO	98.85
GO	56.25
CNT	0
CNT/ZnO	98

GO: graphene oxide; CNT: carbon nanotubes.

Conclusions

The GO/ZnO was successfully synthesized and its performance for photocatalytic degradation of methylene blue was evaluated. A second order model was successfully developed for the photocatalytic process where predicted the process by BBD of the RSM. Analysis of variance showed a high coefficient of determination ($R^2 = 0.95$), thus ensuring a satisfactory adjustment of the second-order regression model with the experimental data. The optimum condition for the removal of methylene blue was resulted at a photocatalyst dosage of 2.1 g L^{-1} , initial pH of 4.5, the H_2O_2 concentration of 3.5×10^{-4} mol L^{-1} and irradiation time of 140 min. Irradiation time and photocatalyst dosage were determined as the most effective factors based on the Pareto analysis, respectively. Under optimum conditions, the other photocatalyst such as ZnO and CNT/ZnO exhibited higher activity in MB decolorization. The study revealed that ZnO/GO could be a promising photocatalyst for decolorization processes.

Acknowledgments

Special thanks to Iranian Nanotechnology Initiative Council for financial supports. The authors wish to thank Prof Ahmad Reza Abbasian, for TEM analysis.

References

- Khataee, A.; Karimi, A.; Soltani, R. D. C.; Safarpour, M.; Hanifehpour, Y.; Joo, S. W.; *Appl. Catal., A* **2014**, *488*, 160.

2. Jantawasu, P.; Sreethawong, T.; Chavadej, S.; *Chem. Eng. J.* **2009**, *155*, 223.
3. Liu, Y.; Hu, Y.; Zhou, M.; Qian, H.; Hu, X.; *Appl. Catal., B* **2012**, *125*, 425.
4. Chen, D.; Wang, D.; Ge, Q.; Ping, G.; Fan, M.; Qin, L.; Bai, L.; Lv, C.; Shu, K.; *Thin Solid Films* **2015**, *574*, 1.
5. Ahmad, M.; Ahmed, E.; Hong, Z. L.; Xu, J. F.; Khalid, N. R.; Elhissi, A.; Ahmed, W.; *Appl. Surf. Sci.* **2013**, *274*, 273.
6. Aia, L.; Zhang, C.; Chena, Z.; *J. Hazard. Mater.* **2011**, *192*, 1515.
7. Bai, S.; Shen, X.; Zhong, X.; Liu, Y.; Zhu, G.; Xu, X.; Chen, K.; *Carbon* **2012**, *50*, 2337.
8. Li, B.; Liu, T.; Wang, Y.; Wang, Z.; *J. Colloid Interface Sci.* **2012**, *377*, 114.
9. Abdullah, A. H.; Jia, H.; Moey, M.; Yusof, N. A.; *J. Environ. Sci.* **2012**, *24*, 1694.
10. Hayat, K.; Gondal, M. A.; Khaled, M. M.; Ahmed, S.; Shemsi, A. M.; *Appl. Catal., A* **2011**, *393*, 122.
11. Rodriguez, L. P.; Cuevas, S. M.; Oller, I.; Agüera, A.; Puma, G. L.; Malato, S.; *J. Hazard. Mater.* **2012**, *211-212*, 131.
12. Baransi, K.; Dubowski, Y.; Sabbah, I.; *Water Res.* **2012**, *46*, 789.
13. Vildoza, D.; Ferronato, C.; Sleiman, M.; Chovelon, J. M.; *Appl. Catal., B* **2010**, *94*, 303.
14. Zhang, W.; Zhang, Q.; Dong, F.; *Ind. Eng. Chem. Res.* **2013**, *52*, 6740.
15. Asl, S. K.; Sadrnezhaad, S. K.; Rad, M. K.; Uner, D.; *Turk. J. Chem.* **2012**, *36*, 121.
16. Khataee, A. R.; Fathinia, M.; Aber, S.; Zarei, M.; *J. Hazard. Mater.* **2010**, *181*, 886.
17. Ray, S.; Lalman, J. A.; Biswas, N.; *Chem. Eng. J.* **2009**, *150*, 15.
18. Tzikalos, N.; Belessi, V.; Lambropoulou, D.; *Environ. Sci. Pollut. Res.* **2013**, *20*, 2305.
19. Azarang, M.; Shuhaimi, A.; Yousefi, R.; Golsheikh, A. M.; Sookhakian, M.; *Ceram. Int.* **2014**, *40*, 10217.
20. Lv, T.; Pan, L.; Liu, X.; Lu, T.; Zhu, G.; Sun, Z.; *J. Alloys Compd.* **2011**, *509*, 10086.
21. Hummers, W. S.; Offeman, R. E.; *J. Am. Chem. Soc.* **1958**, *80*, 1339.
22. Kumar, S. S.; Venkateswarlu, P.; Rao, V. R.; Rao, G. N.; *Int. Nano Lett.* **2013**, *3*, 30.
23. Wang, Y.; Liu, J.; Liu, L.; Sun, D. D.; *J. Nanosci. Nanotechnol.* **2012**, *12*, 3896.
24. Rahman, M. M.; Adil, M.; Yusof, A. M.; Kamaruzzaman, Y. B.; Ansary, R. H.; *Materials* **2014**, *7*, 3634.
25. Cobas, M.; Sanromán, M. A.; Pazos, M.; *Bioresour. Technol.* **2014**, *160*, 166.
26. Liu, H. L.; Chiou, Y. R.; *Chem. Eng. J.* **2005**, *112*, 173.
27. Khataee, A. R.; Zarei, M.; *Desalination* **2011**, *278*, 117.
28. Khataee, A. R.; Zarei, M.; Fathinia, M.; Jafari, M. K.; *Desalination* **2011**, *268*, 126.

Submitted: March 17, 2016

Published online: June 9, 2016